AL KINDI M., PICKFORD M., GOMMERY D. & QATAN A. (2020). Stratigraphy, palaeoclimatic context and fossils of the southern Rub al Khali (the Empty Quarter): geological-surveying results of a geo-archaeological survey around the area of Maintan in the Sultanate of Oman. *Historical Biology*. doi.org/10.1080/08912963.2020.1717485

ANNEXE

FIGURES

Figure 1. Satellite Map of Oman showing the study area in the south-eastern side of the Rub Al Khali, between 280-300 metres above sea-level. (© AL KINDI M., PICKFORD M., GOMMERY D. & QATAN A.)

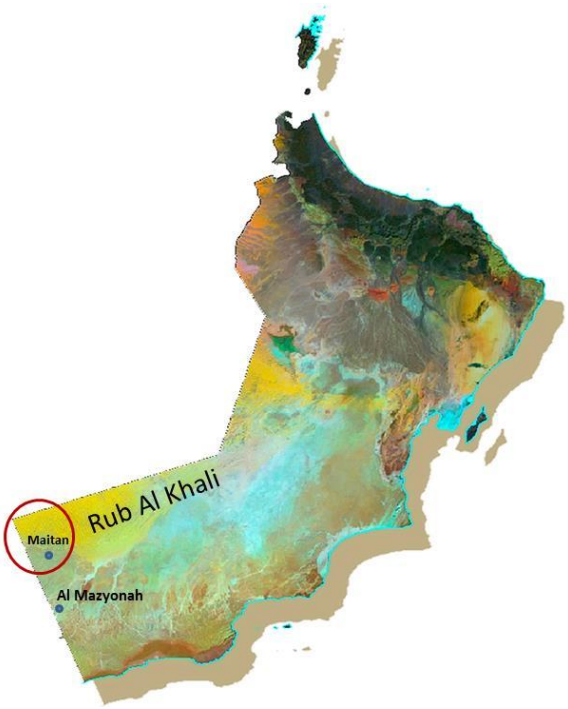

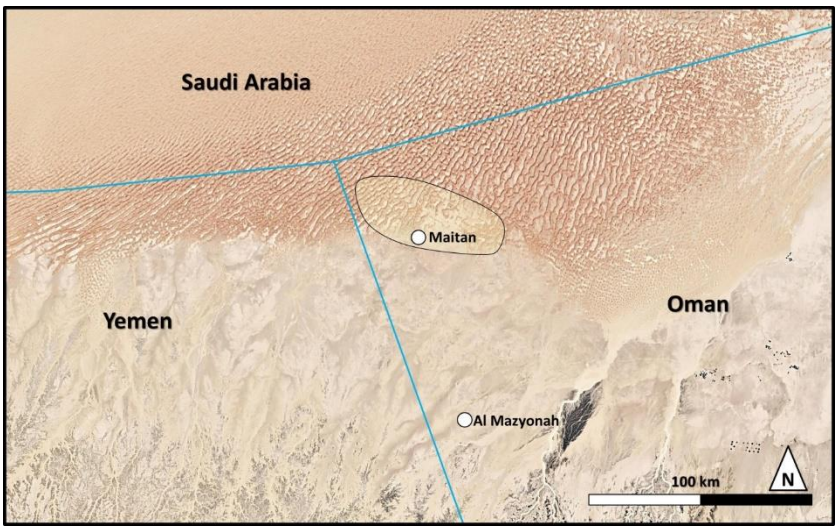

Figure 2. The study area (shaded here in yellow) is located north of the Village of Maitan in the triple border junction between Oman and both Yemen and Saudi Arabia. Detailed observations were mostly focused on the western side of this shaded zone. The satellite image is modified from Google Earth. (© AL KINDI M., PICKFORD M., GOMMERY D. & QATAN A.)

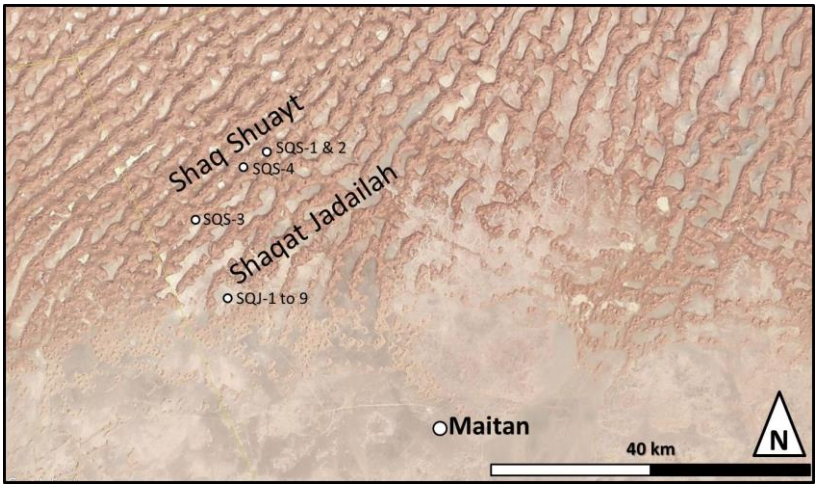

Figure 3. The locations of Shaq Shuayt and Shaqat Jadailah in Uruq Al Hadd Linear Sand Dunes north of Maitan. The satellite image is modified from Google Earth. (© AL KINDI M., PICKFORD M., GOMMERY D. & QATAN A.)

Figure 4. The main sites in Shaqat Jadailah (SQJ), where the greatest concentration of Neolithic artefacts was found and where most of the surveying efforts were focused. These sites are located within a large bowl that could be easily accessed only through two narrow zones in the NW and SW. The silty gypsum mounds and flats in the bowl as well as the tufa deposits indicate the presence of ancient springs in this area. The silty gypsum deposits mostly appear white in this satellite image, these are often associated with tufa deposits, whereas the consolidated sand dunes are often located on the flanks of the existing large sand dunes in the area. SQJ-2 was the first site reported by local people, where grind stones and mills were found. The satellite image is modified from Google Earth. (© AL KINDI M., PICKFORD M., GOMMERY D. & QATAN A.)

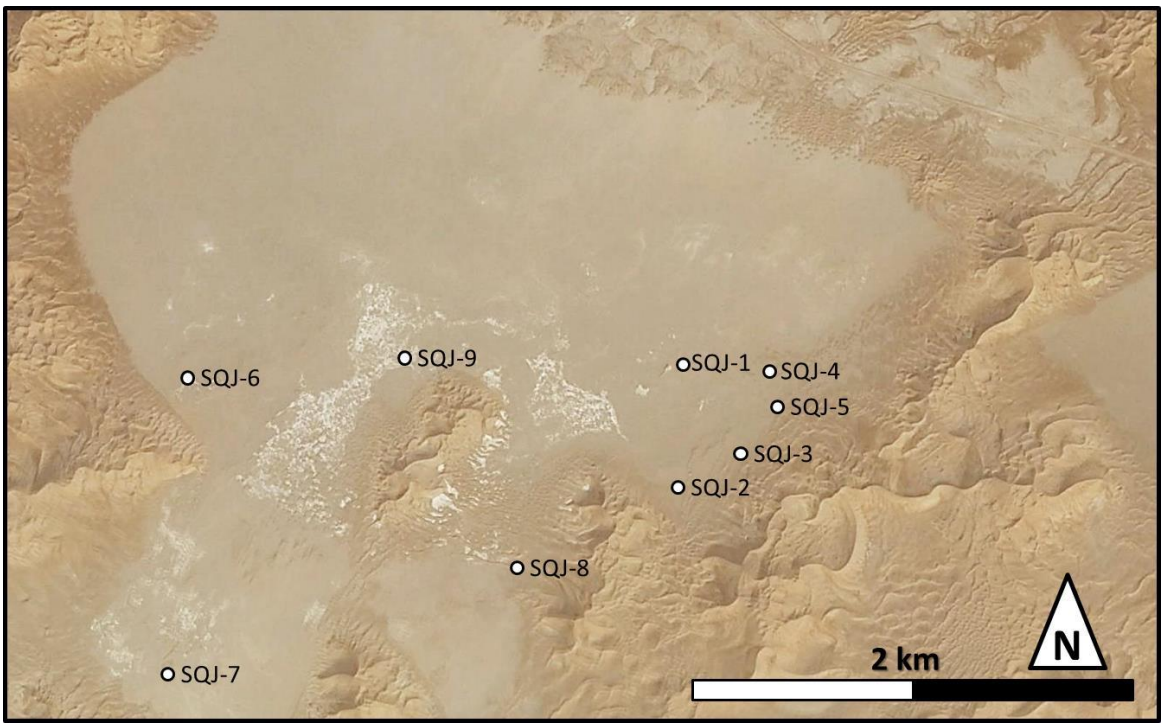

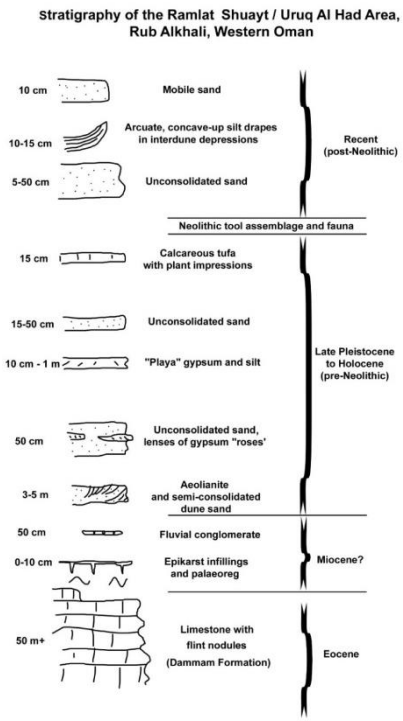

Figure 5. A schematic section representing the stratigraphy of the Uruq Al Hadd Area, Rub Al Khali, Western Oman, the section is combined from various smaller sections in the area of interest. (© AL KINDI M., PICKFORD M., GOMMERY D. & QATAN A.)

Figure 6. White marine limestone of the Dammam Formation overlain by epikarst fissure infillings and unconsolidated sand, 6.2 km due east of Maitan. Note the complex linear dunes in the background and the vegetation that covers the area. (© AL KINDI M., PICKFORD M., GOMMERY D. & QATAN A.)

Figure 7. Both the white Eocene limestone and the chert nodules within them provided raw materials for the manufacture of lithic tools during the Palaeolithic and Neolithic in the area around Maitan (Scale bar is 20 cm). (© AL KINDI M., PICKFORD M., GOMMERY D. & QATAN A.)

Figure 8. Cemented sand and pebbles infilling epikarst fissures developed in the Dammam Formation limestone, 6.2 km east of Maitan. Some of these features are pre-existing faults, as noted from the small displacement across their planes, which acted as fluid-conduit planes from the underlying artesian aquifers. (© AL KINDI M., PICKFORD M., GOMMERY D. & QATAN A.)

Figure 9. Cemented red sand and conglomerate of fluvial origin, 15 km north-north-west of Maitan, tentatively correlated to the Shisr Formation or Marsawdad Formation of possible Miocene-Pliocene age. (© AL KINDI M., PICKFORD M., GOMMERY D. & QATAN A.)

Figure 10. Consolidated aeolianite north of Maitan, the thickness of the aeolianite varies from place to place and the eroded surface on top of it can be richly endowed with Neolithic tools, ornaments and some fauna. (© AL KINDI M., PICKFORD M., GOMMERY D. & QATAN A.)

Figure 11. Areally extensive but thin gypsiferous silty « playa » deposits (sabkha) with polygonal shrinkage cracks occur widely in the interdune « Urg or Shaq » of the Rub Al Khali. These deposits are seldom more than a metre thick. (© AL KINDI M., PICKFORD M., GOMMERY D. & QATAN A.)

Figure 12. Semi-consolidated, well-bedded aeolian sand cemented by gypsum and overlain by remnants of a mound of gypsiferous silt/clay (SQJ-2). (© AL KINDI M., PICKFORD M., GOMMERY D. & QATAN A.)

Figure 13. Dark brown sand with « desert roses » associated with pale gypsum deposits. The height of the gypsum structure is about 40 cm. These « desert roses » (sandy gypsum crystals) occur in the sands beneath widespread gypsiferous clay/silt deposits (Site SQJ-6). (© AL KINDI M., PICKFORD M., GOMMERY D. & QATAN A.)

Figure 14. Gypsiferous clay/silt mound with rhizoliths overlying semi-consolidated aeolian sand (SQJ-1). (© AL KINDI M., PICKFORD M., GOMMERY D. & QATAN A.)

Figure 15. Gypsiferous clay/silt mound overlying semi-consolidated aeolian sand and a large bifacial tool with adhering gypsum crust (inset) (near SQJ-4). These mounds could represent the sites of springs (scale bar in the inset photo is 5 cm). (© AL KINDI M., PICKFORD M., GOMMERY D. & QATAN A.)

Figure 16. Circular, concave-up silt drape overlying unconsolidated dune sand, 40 km north-north-east of Maitan, the result of a single rain storm flooding an interdune depression, with subsequent removal of the adjacent dune by aeolian activity and sand deposition within the depression leaving the raised edges emergent. These deposits tend to be eroded rapidly and may disappear within a few years of their formation. (© AL KINDI M., PICKFORD M., GOMMERY D. & QATAN A.)

Figure 17. Immense linear dunes cover about 50 % of the land surface in the Rub Al Khali. Overall, the dunes are relatively immobile, but their surface topography changes on a daily basis. Shown is a limb of a large star dune, part of a linear dune complex more than 50 km long. The interdune area in the middle is part of the Shaq Shuayt interdunal system, where a concentration of Late Palaeolithic tools occurs. (© AL KINDI M., PICKFORD M., GOMMERY D. & QATAN A.)

Figure 18. Large cowrie shell, *Cypraea grayana*, from SQJ-8, utilised as an ornament (dorsal part removed). A) stereo ventral view, B) stereo dorsal view (note the thin coating of aeolianite inside the shell) (scale: 10 mm). (© AL KINDI M., PICKFORD M., GOMMERY D. & QATAN A.)

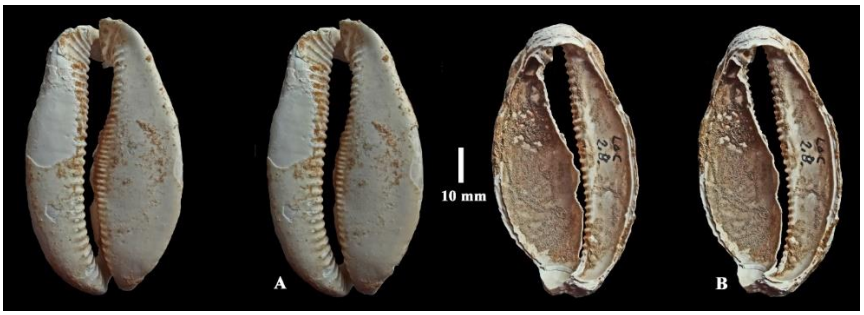

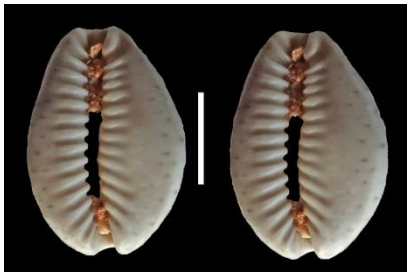

Figure 19. Small *Cypraea* shell, stereo ventral view, utilised as an ornament (dorsal part removed) from SQJ-2 (scale: 10 mm). (© AL KINDI M., PICKFORD M., GOMMERY D. & QATAN A.)

Figure 20. Stereo views of small marine snails from SQJ-8, some of which are coated and infilled with indurated dune sand. A-D) *Cypraea* spp. shells, E) Indeterminate dorsal part of shell, F) eroded *Morula granulata* (1 - dorsal views; 2 - ventral views) (scale: 10 mm). (© AL KINDI M., PICKFORD M., GOMMERY D. & QATAN A.)

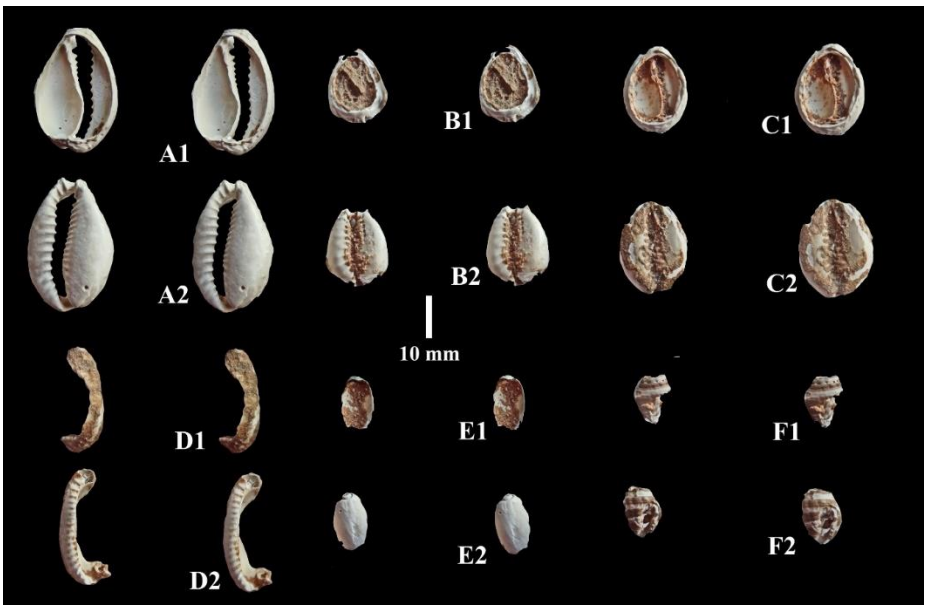

Figure 21. Stereo images of marine shells associated with Neolithic implements at SQJ-8. A) *Cypraea* sp. (A1 - ventral view, A2 - dorsal view); B) *Oliva bulbosa*, (B1 - ventral view, B2 - dorsal view); C) oblong wedge of ribbed bivalve, probably *Chlamys* sp. (C1 - outer surface, C2 - inner surface) (scale: 10 mm). (© AL KINDI M., PICKFORD M., GOMMERY D. & QATAN A.)

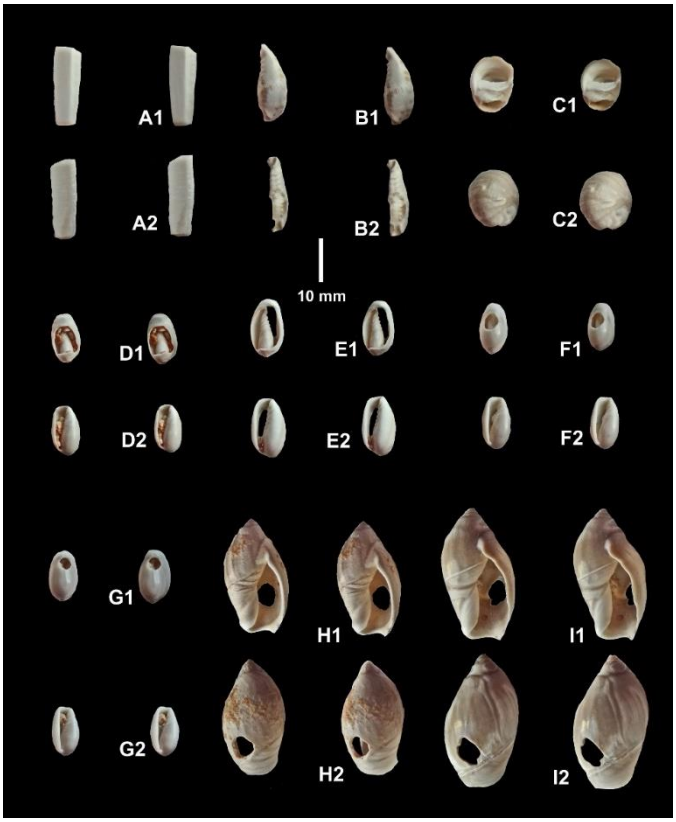

Figure 22. Stereo views of marine molluscs from SQJ-2. A) oblong wedge of bivalve shell, B) fragment of *Cypraea* sp. C) *Nerita textilis*, D-G) *Volvarina* spp. H-I) *Ancilla ovalis* (1 - dorsal views, 2 - apertural views except for C1 and C2 and I1 and I2 which are apertural and dorsal views respectively) (scale: 10 mm). (© AL KINDI M., PICKFORD M., GOMMERY D. & QATAN A.)

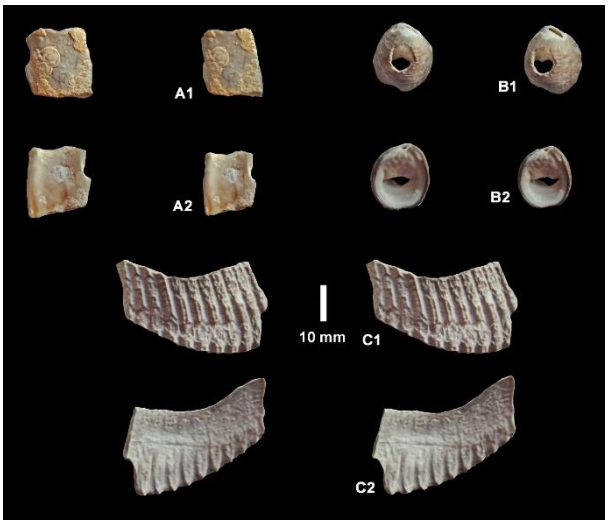

Figure 23. Stereo images of seashells Urq Shuayt.A) fragment of degraded nacrous bivalve shell (1 - outer surface, 2 - inner surface); B) *Nerita albicilla*, (1 - dorsal view, 2 - ventral view); C) *Chlamys* sp. (1 - outer surface, 2 - inner surface) (scale: 10 mm). (© AL KINDI M., PICKFORD M., GOMMERY D. & QATAN A.)

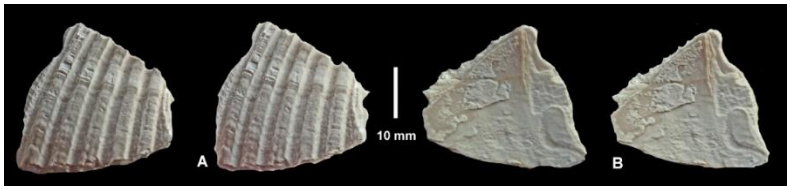

Figure 24. Stereo views of a shell fragment of *Chlamys* from SQJ-2. A) outer surface, B) inner surface (scale: 10 mm). (© AL KINDI M., PICKFORD M., GOMMERY D. & QATAN A.)

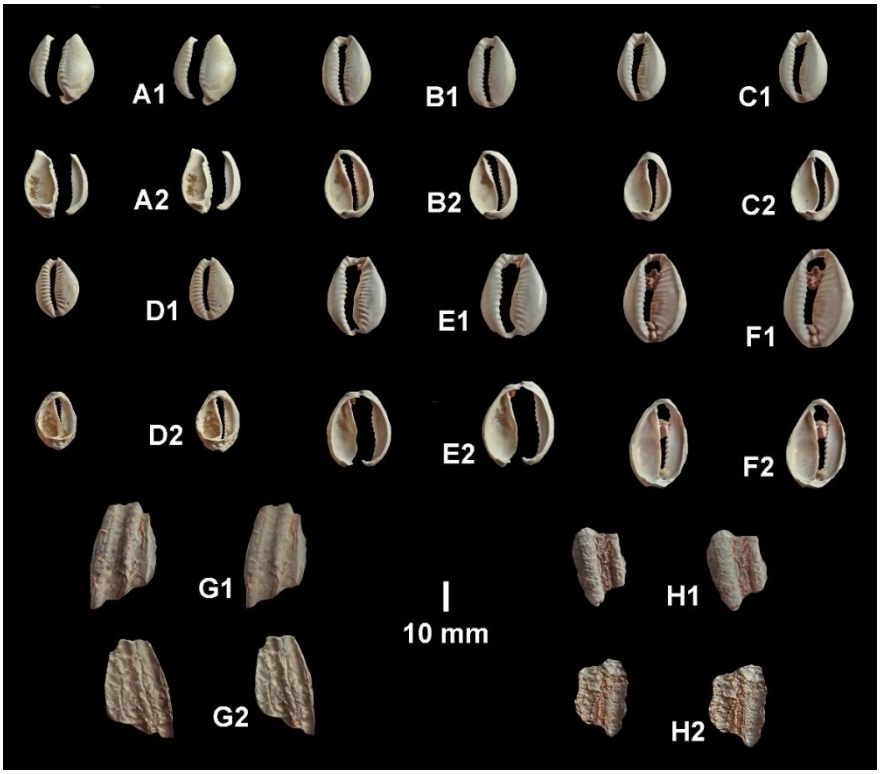

Figure 25. Stereo images of cypraeids and bivalve shells near SQJ-4. A-F) *Cypraea* spp. (1 - ventral views, 2 - dorsal views) A and E are broken; G-H) fossil *Chlamys* sp. (1 - outer surfaces, 2 - inner surfaces) (scale: 10 mm). (© AL KINDI M., PICKFORD M., GOMMERY D. & QATAN A.)

Figure 26. Stereo images of a button-like object manufactured from a marine bivalve shell, possibly *Anadara* sp. from the area near SQJ-4. (A - outer surface, B - inner surface) (scale: 10 mm). (© AL KINDI M., PICKFORD M., GOMMERY D. & QATAN A.)

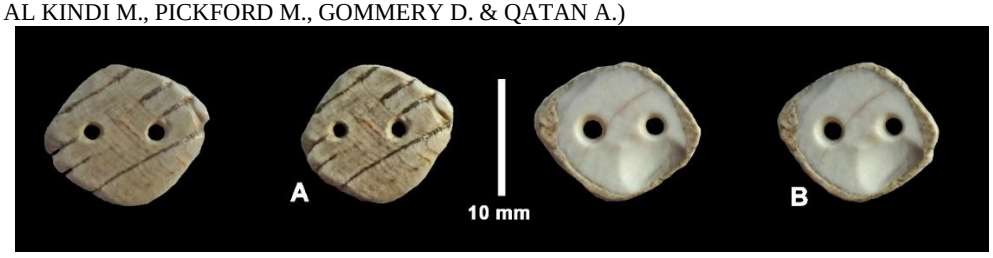

Figure 27. Stereo images of a bead from the area near SQJ-4, made from a small fossilised sea urchin. A) ventral view, B) dorsal view (scale: 10 mm). (© AL KINDI M., PICKFORD M., GOMMERY D. & QATAN A.)

Figure 28. Stereo views of an ornament made from a fragment of bivalve shell. A) outer side (note shallow linear groove worn between the two notches and the vertical shell microstructure), B) inner view (note the horizontal shell microstructure and a sinuous ridge traversing from top to bottom in the middle of the object) (scale: 10 mm). (© AL KINDI M., PICKFORD M., GOMMERY D. & QATAN A.)

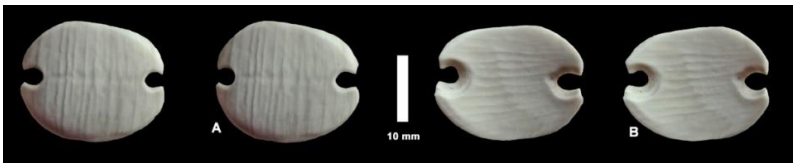

Figure 29. Eggshell fragment from locality SQJ-2.5 which is 2.6 mm thick, possibly representing the extinct ostrich species *Diamantornis laini*, A) strongly eroded/dissolved outer surface, B) slightly dissolved inner surface (scale: 10 mm). (© AL KINDI M., PICKFORD M., GOMMERY D. & QATAN A.)

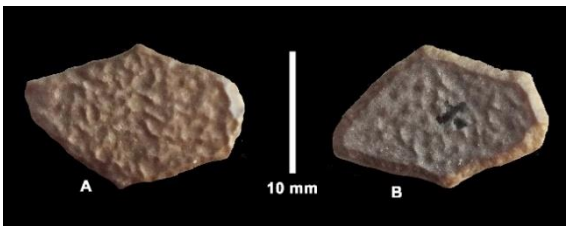

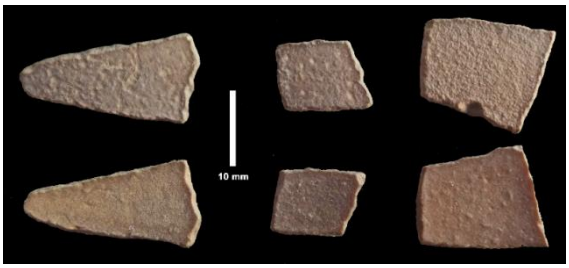

Figure 30. Fossil eggshell fragments from SQJ-1, attributed to *Struthio camelus*. Top row - external surface, bottom row - internal surface (scale: 10 mm). (© AL KINDI M., PICKFORD M., GOMMERY D. & QATAN A.)

Figure 31. Fossil eggshell fragments from SQJ-8, attributed to *Struthio camelus*. A) stereo views of external surface to show the pores, B) internal surface (scale: 10 mm). (© AL KINDI M., PICKFORD M., GOMMERY D. & QATAN A.)

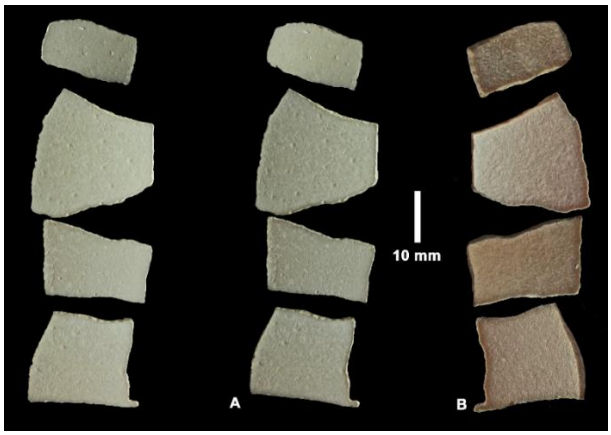

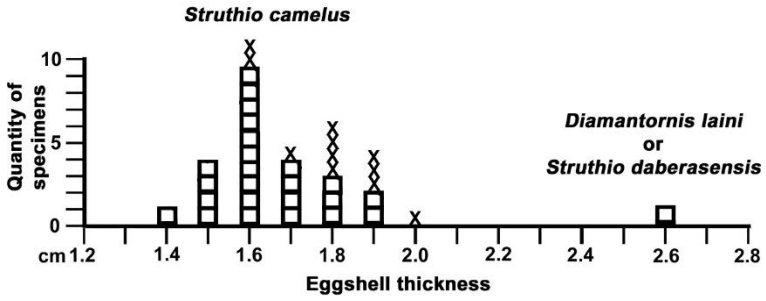

Figure 32. Univariate plots of struthious eggshell thickness. Only unweathered specimens were measured. Squares - unworked fragments, X - perforated eggshells. There is a clear preference to use thicker shells to manufacture beads. (© AL KINDI M., PICKFORD M., GOMMERY D. & QATAN A.)

Figure 33. Beads manufactured from ostrich eggshell, locality SQJ-2.9, Uruq Al Hadd. The doubly perforated button in the lower row at the left is made from a marine shell (see Fig. 10) (scale bar: 5 cm). (© AL KINDI M., PICKFORD M., GOMMERY D. & QATAN A.)

Figure 34. Bead shapers or arrow shaft straighteners made from limestone pebbles found in the area near SQJ-4 provide evidence that Neolithic people in Uruq Al Hadd may have manufactured their beads on site. (© AL KINDI M., PICKFORD M., GOMMERY D. & QATAN A.)

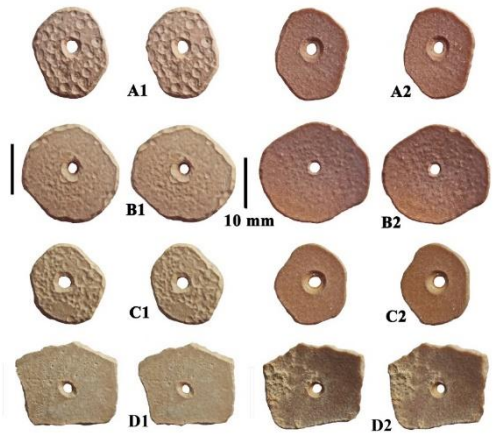

Figure 35. Stereo views of beads from the area near SQJ-4 manufactured from fossilised ostrich eggshell fragments. In A-C, the outer surfaces of the eggshells were partly dissolved before drilling took place, and some dissolution occurred after the beads were completed. In unfinished bead D, the inner surface of the eggshell has aeolianite adhering to it which has been drilled through by the bead maker, 1) outer surface, 2) inner surface (scale: 10 mm). (© AL KINDI M., PICKFORD M., GOMMERY D. & QATAN A.)

Figure 36. Stereo views of a relatively unweathered ostrich eggshell bead from Uruq Al Hadd, Oman, outer (left) and inner (right) surfaces (scale: 10 mm). (© AL KINDI M., PICKFORD M., GOMMERY D. & QATAN A.)

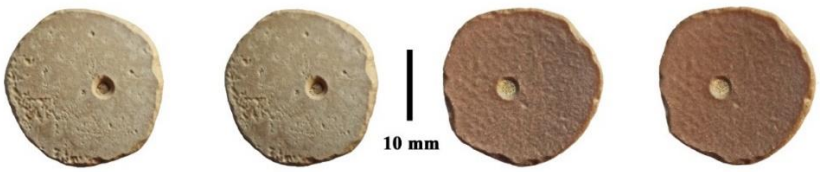

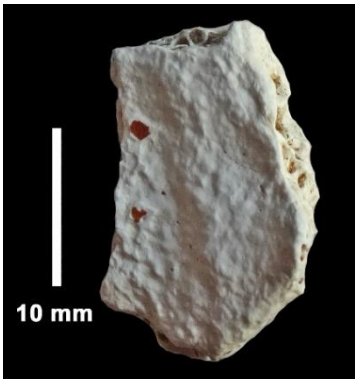

Figure 37. Chelonian scute from locality SQJ-2.9, Uruq Al Hadd, Rub Al Khali, Oman (scale: 10 mm). (© AL KINDI M., PICKFORD M., GOMMERY D. & QATAN A.)

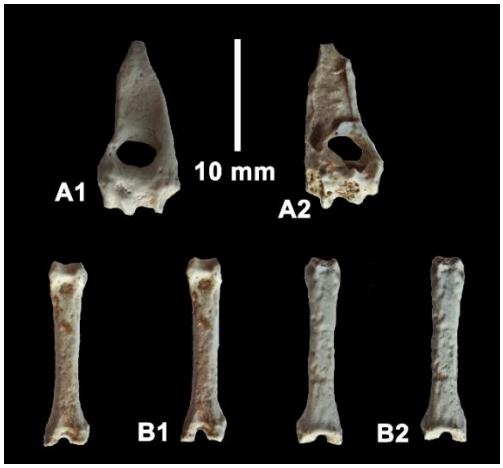

Figure 38. Lagomorph remains from Neolithic context, Uruq Al Hadd, Oman. A) distal humerus from locality SQJ-2.9 (A1 - caudal view, A2 - cranial view), B) stereo views of first phalanx from locality SQJ-1.2 (B1 - volar view, B2 - dorsal view) (scale: 10 mm). (© AL KINDI M., PICKFORD M., GOMMERY D. & QATAN A.)

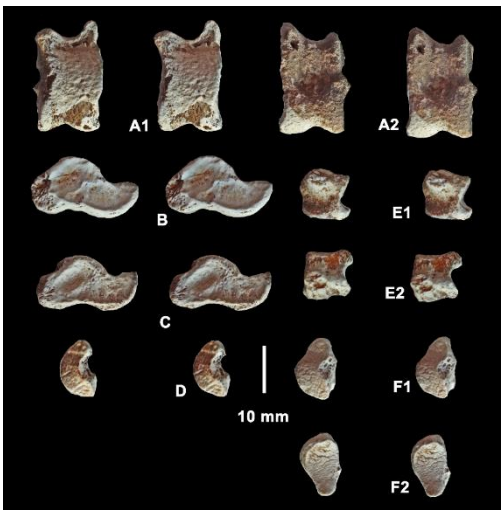

Figure 39. Small bovid remains from Neolithic sites in the Uruq Al Hadd. A) right talus from SQJ-2, B) right talus from SQJ-4, C) right talus from SQJ-4, D) cuneiform C3 from SQJ-4, E) scaphoid from SQJ-2, F) cuneiform C3 from SQJ-2 (scale: 10 mm). (© AL KINDI M., PICKFORD M., GOMMERY D. & QATAN A.)

Figure 40. Bivariate plot (external length: distal breadth) of bovid tali from Oman. The arrows show the lengths of incomplete fossil specimens. The grey oval for Neolithic specimens is estimated on the basis of the relation between external length and distal breadth of ruminant tali in general. The Neolithic specimens are clearly all smaller than the range of variation found in extant Omani goats and sheep. (© AL KINDI M., PICKFORD M., GOMMERY D. & QATAN A.)

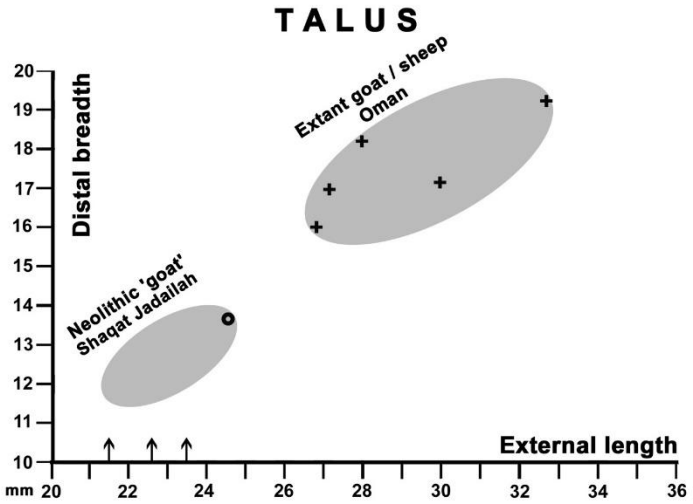

Figure 41. The formation of interdunal desert lakes in the eastern side of Rub Al Khali, following the cyclonic storm Mekunu that struck south-eastern Oman (Dhofar) at the end of May, 2018, covering great parts of eastern Rub Al Khali with a green lush that lasted a few months after the storm (Courtesy: Ahmed Al Touqi).

Figure 42. A large mound between SQJ-1 and SQJ-2 consists of semi-consolidated dune sand at the base, capped by a layer of gypsum nearly 1 metre thick. This could be the site of a former spring, now isolated as a mesa by erosion of the surrounding weakly consolidated sands. Neolithic artefacts occur on the top of the gypsum deposits, one being found attached to the gypsum.

TABLES

Table 1. Terrestrial faunal remains associated with Neolithic tools in Uruq Al Hadd, 2019 collection (the numbers refer to quantity of fragments collected). (© AL KINDI M., PICKFORD M., GOMMERY D. & QATAN A.)

SQJ-1	SQJ-2	SQJ-3	SQJ-4	SQJ-5	SDS-1	SDS-2
***Struthio camelus* (73)**	*Struthio camelus* (2)	*Struthio camelus* (40)	*Struthio camelus* (11)	*Struthio camelus* (17)	*Struthio camelus* (8)	*Struthio camelus* (46)
		Diamantornis laini / Struthio daberasensis (1)				
				Chelonian (2)		
	Lagomorph sp. (1)			Lagomorph sp. (1)		
	cf *Capra* sp. (4)			cf *Capra* sp. (3)		
	Medium ruminant (6)					

Table 2. Measurements (in mm) of fossil lagomorph bones from the Neolithic site at Uruq Al Hadd, Oman. (© AL KINDI M., PICKFORD M., GOMMERY D. & QATAN A.)

Locality	Bone	Length	Proximal breadth	Proximal height	Distal breadth	Distal height
SQJ-2.9	Humerus	--	--	--	7.0	5.0
SQJ-1.2	1st phalanx	16.5	4.0	3.1	3.1	2.4

Table 3. Measurements (in mm) of small bovid tali from Oman. Fossils are from the Neolithic sites in the Uruq Al Hadd, the modern specimens are goats/sheep from Wadi Al Banah in North Oman. (© AL KINDI M., PICKFORD M., GOMMERY D. & QATAN A.)

Locality	Bone	External length	Internal length	Proximal breadth	Distal breadth	Distal height
SQJ-2	Rt talus	24.6	22.6	13.0	13.7	12.8
SQJ-2	Lt talus	23.5	--	--	--	--
SQJ-4	Rt talus	22.6	--	--	--	--
SQJ-4	Rt talus	21.6	--	--	--	--
Modern	Lt talus	30.0	27.6	17.6	18.2	13.2
Modern	Rt talus	28.8	27.0	17.0	18.2	12.7
Modern	Rt talus	27.2	25.6	15.4	16.0	12.0
Modern	Lt talus	26.8	25.2	15.4	16.0	12 .0
Modern	Lt talus	32.7	31.0	18.4	19.1	--

Table 4. Measurements (in mm) of post-cranial elements of bovids associated with Neolithic implements at Uruq Al Hadd, Oman. (© AL KINDI M., PICKFORD M., GOMMERY D. & QATAN A.)

Locality	Bone	Breadth	Proximo-distal height
SQJ-1.2	Scaphoid	5.9	9.9
SQJ-1.2	Cuneiform C3	12.2	4.5
SQJ-2.9	Cuneiform C3	12.0	4.3